Understanding Si adsorption on GaN(0001) surfaces using first-principles calculations

A. L. Rosa*
Uppsala University, Department of Physics, Box 530, 75121, Uppsala, Sweden

J. Neugebauer
Max-Planck-Institut für Eisenforschung, Max-Planck-Strasse 1, 40237, Düsseldorf, Germany
(Received 7 September 2005; revised manuscript received 17 January 2006; published 9 May 2006)

We report in detail the results of our first-principles investigations of Si adsorption on GaN(0001) surfaces which were briefly presented in an earlier publication [Appl. Phys. Lett. **80**, 2008 (2002)]. We employ density-functional theory within the local-density approximation to investigate Si adsorption on GaN(0001) surfaces with (1×1), (2×2), and $(\sqrt{3}\times\sqrt{3})R30°$ reconstructions. We find that adsorption at subsurface sites is energetically favorable compared to adsorption on the top layers. In particular, we find that under Ga-rich conditions a Ga bilayer is formed on the top of a Ga-terminated surface with Si incorporated underneath. Under such conditions Si does not affect the GaN surface morphology. Under both N-rich and Si-rich conditions, an N-terminated structure with Si in the second layer is preferred, leading to rough surfaces.

DOI: 10.1103/PhysRevB.73.205314 PACS number(s): 73.20.At, 71.15.Mb

I. INTRODUCTION

The group-III nitrides (AlN, GaN, and InN) represent an important class of semiconductors because of their direct band gaps which span the range 0.7–6.2 eV, including the visible and ultraviolet regions of the spectrum.[2] In particular, GaN has a band gap of 3.4 eV at room temperature and has been by far the most intensively studied material among the group-III nitrides. The most common growth direction of epitaxial hexagonal GaN is normal to the {0001} basal plane (see, for example, Ref. 3 and references therein). It is important to note that the (0001) (or Ga-polar) and $(000\bar{1})$ (or N-polar) directions are not equivalent and exhibit different properties. The structural and electronic properties of GaN surfaces depend sensitively on the orientation of the surface, surface termination, and reconstruction.[4–8]

The GaN(0001) surfaces have been demonstrated to have a better surface morphology and are therefore the relevant surfaces for technological applications.[2] Depending on the growth conditions the GaN(0001) surface exhibits a large variety of reconstructions, such as (1×1), (2×2), (4×4), (5×5), and (6×4).[9–13]

Intentionally *n*-type doping in GaN is usually achieved using Si as dopant. Although incorporation of Si in GaN bulk has been extensively investigated from both theoretical[14,15] and experimental[16,17] points of view, a clear understanding on how Si affects GaN surfaces is still missing.

Metal-organic chemical vapor deposition (MOCVD) and metal-organic vapor phase epitaxy (MOVPE) studies reported that Si concentrations in the range of 10^{18}–10^{19} cm^{-3} modify the GaN growth from a step-flow mode to three-dimensional growth. At higher concentrations it might even lead to formation of quantum dots (QD's).[18]

MOCVD growth has also shown that Si concentrations above 1×10^{19} cm^{-3} induce roughness[19] and crack formation.[20,21] At low-temperature MOCVD growth (around 1070 K), Si adsorption leads to smooth surfaces even for high Si concentrations (3×10^{19} cm^{-3}).[22] In the latter case, the adsorption of Si appeared to change the surface mobility of the Ga species, resulting in a larger average terrace length. Munkholm *et al.*[23] have also reported that at concentrations above 2×10^{19} cm^{-3} Si segregates to the surface and changes the growth mode from step flow to layer by layer over a large range of growth temperatures (890–1220 K).

On the other hand, Si doping on GaN surfaces by molecular-beam epitaxy (MBE) has been shown to lead to smooth surfaces. Depositing Si on a unreconstructed surface (1×1) is found to have no discernable effect on the surface reconstruction. In contrast, by depositing between 1/4 and 1/2 monolayers (ML) of Si on the (5×5) GaN(0001) surfaces, a (2×2) reconstruction is observed. With increasing substrate temperature the (2×2) disappears, implying that the (2×2) structure is metastable. The (5×5) reconstruction still covers some regions of the surface. With additional $\frac{1}{4}$ ML, the (1×1) starts to cover the entire surface.[1]

We can see from the reported experimental results that there is no clear understanding of the role of Si on GaN surfaces. Therefore, in order to clarify how Si affects the GaN morphology and explain why under certain conditions Si does not change the surface morphology whereas under other conditions it promotes rough surfaces, we have performed density-functional theory calculations. Here we include a detailed description of our results briefly reported in Ref. 1, including the atomic and thermodynamic properties of various reconstructed and unreconstructed surfaces.

Our paper is organized as follows. In Sec. II we give a description of the computational details. In Sec. III we discuss our results for Si incorporation in GaN bulk and on GaN(0001) surfaces. Then in Sec. III D we discuss our results for Si adsorption on clean GaN(0001) surfaces. Finally, in Sec. IV we conclude.

II. METHODOLOGY

In this work we employ density-functional theory[24,25] in the local-density approximation[26] as parametrized by Perdew and Zunger[27] to study Si adsorption on GaN(0001) surfaces. We use norm-conserving, nonlocal pseudopotentials gener-

ated within the Troullier-Martins scheme.[28,29] For Ga we use the configuration $3d^{10}4p^24p^1$ and the cutoff radii $r_s=2.08$ bohrs, $r_p=2.30$ bohrs, and $r_d=2.08$ bohrs, treating the s as local component to avoid ghost states. For N we use the configuration $2s^22p^23d^0$ with the following cutoff radii: $r_s=1.5$ bohr, $r_p=1.5$ bohr, and $r_d=1.5$ bohr and the s component as the local component. Those pseudopotentials have been successfully used to describe bulk properties GaN.[30] The electron wave functions are expanded in a plane-wave basis set using a 70-Ry cutoff energy. The surfaces are treated using periodically repeated slabs with nine layers of GaN and 11 Å of the vacuum region, where one side of the slab is saturated with hydrogen atoms of fractional charge $0.75e^-$. Surface unit cells with (1×1), $(\sqrt{3}\times\sqrt{3})$, and (2×2) periodicity were employed, with Monkhorst-Pack[31] meshes of $(4\times4\times1)$, $(3\times3\times1)$, and $(2\times2\times1)$ special **k** points for the Brillouin zone integration, respectively. The top three to five layers of the surface were allowed to relax until the forces on the atoms were smaller than 10^{-4} eV/Å. For GaN bulk, Si, Ga bulk, and $\beta-Si_3N_4$, 33, 10, 216, and 63 **k** points in the irreducible Brillouin zone were used, respectively. For the calculation of the N_2 molecule and N atom we use a cubic supercell with length $L=10$ Å and 1 **k** point.

We calculate Si incorporation in GaN bulk, where Si replaces a Ga atom (Si_{Ga}). Configurations with Si at interstitial positions or at the N site have been found to be energetically unfavorable.[15] This can be understood considering that Si has an atomic radius (1.1 Å) very similar to Ga (1.26 Å). On the other hand, Si on the N site or interstitially causes a large strain, because Si has a much larger atomic radius than N (0.75 Å). The calculations were performed using a supercell with 64 atoms containing one defect per cell. In thermodynamic equilibrium the dopant concentration is given by

$$C = N_{\text{sites}} e^{-\Delta G_f/k_BT} = 4.4\times10^{22}\ \text{cm}^{-3}\ e^{-\Delta E_f/k_BT}, \quad (1)$$

where k_B is the Boltzmann constant, T is the temperature, and N_{sites} is the number of sites in the crystal where the defect can be. ΔG_f is the defect formation energy, and it is given by

$$\Delta G_f = \Delta E_f - T\Delta S_f + P\Delta V_f. \quad (2)$$

ΔE_f is the change in the total energy, ΔS_f is the change in the vibrational entropy, and ΔV_f is the change in the volume when the defect is introduced in the system. Here we will not consider changes in the volume and entropy, since they are considered to be small. The defects formation energies will be defined with respect to external chemical potentials for the various species involved. The formation energy of a Si substitutional in GaN will be then calculated as

$$\Delta E_f = E_{\text{tot}}^{\text{GaN bulk}}(\text{Si}_{\text{Ga}}) - E_{\text{tot}}^{\text{GaN bulk}} - \mu_{\text{Si}} + \mu_{\text{Ga}}, \quad (3)$$

where $E_{\text{tot}}^{\text{GaN bulk}}(\text{Si}_{\text{Ga}})$ and $E_{\text{tot}}^{\text{GaN bulk}}$ are the total energy of GaN bulk with and without defect, respectively. Assuming thermodynamic equilibrium, the N and Ga chemical potentials are not independent, but related by $\mu_{\text{GaN}}=\mu_{\text{Ga}}+\mu_{\text{N}}$, where μ_{GaN} is the GaN chemical potential. Another condition is that the chemical potential for each species must be smaller than the chemical potential of the corresponding elementary phase. Thus we have

$$\mu_{\text{Ga}} \leqslant \mu_{\text{Ga bulk}}, \quad \mu_{\text{N}} \leqslant \mu_{\text{N}_2\ \text{molecule}}. \quad (4)$$

As the formation enthalpy ΔH_f of GaN is given by

$$\Delta H_f^{T=0} = E_{\text{tot}}^{\text{GaN bulk}} - E_{\text{tot}}^{\text{Ga bulk}} - E_{\text{tot}}^{\text{N}_2\ \text{molecule}}, \quad (5)$$

by combining Eqs. (4) and (5) we obtain the range of thermodynamically allowed chemical potentials for N and Ga,

$$\Delta H_f^{T=0} \leqslant \mu_{\text{N}} - \mu_{\text{N}_2\ \text{molecule}} \leqslant 0 \quad (6)$$

and

$$\Delta H_f \leqslant \mu_{\text{Ga}} - \mu_{\text{Ga bulk}} \leqslant 0. \quad (7)$$

For Si in GaN bulk, the following phases can limit the solubility: Si can form droplets on the surface or diffuse into the bulk, forming silicon-nitrogen and/or silicon-gallium compounds. We assume that the Si chemical potential is imposed to obey the lower bound

$$\mu_{\text{Si}} \leqslant \mu_{\text{Si bulk}}. \quad (8)$$

Several silicon-nitrogen compounds are known, Si_3N_4 being a very stable one. We will consider it as the upper bound, so that

$$3\mu_{\text{Si}} + 4\mu_{\text{N}} \leqslant \mu_{\text{Si}_3\text{N}_4}. \quad (9)$$

Combining Eqs. (8) and (9), we obtain that the limit under N-rich conditions is

$$\mu_{\text{Si}} - \mu_{\text{Si bulk}} = \frac{1}{3}\Delta H_f^{\text{Si}_3\text{N}_4} \quad (10)$$

and under Ga-rich conditions

$$\mu_{\text{Si}} - \mu_{\text{Si bulk}} = \frac{1}{3}\Delta H_f^{\text{Si}_3\text{N}_4} - \frac{4}{3}\Delta H_f^{\text{GaN}}. \quad (11)$$

TABLE I. Calculated and experimental structural and thermodynamic properties of α-GaN using the local density approximation (LDA): equilibrium lattice constants a_0, c_0/a_0 ratio, internal parameter u, bulk modulus B_0, cohesive energy E_{coh}, and formation enthalpy $\Delta H_f^{T=0}$. The cohesive energy was corrected by a spin-polarization correction of 0.145 eV (taken from Ref. 36).

Ref.	a_0 (Å)	c_0/a_0	u	B_0 (Mbar)	E_{coh} (eV)	$\Delta H_f^{T=0}$ (eV)
This work	3.196	1.631	0.375	1.87	−10.40	−1.25
33 (Expt.)	3.189	1.624	0.375	1.88	−9.06	−1.15

TABLE II. Calculated structural and thermodynamic properties of Si bulk using the LDA: equilibrium lattice constant a_0, bulk modulus B_0, and cohesive energy E_{coh}. The spin-polarization correction for the Si atom is 0.66 eV. This value was taken from Ref. 36.

Ref.	a_0 (Å)	B_0 (MBar)	E_{coh} (eV)
This work	5.38	0.95	−5.18
34 (Expt.)	5.43	0.98	−4.63

The cohesive energies of the GaN bulk, Ga bulk, $\beta-Si_3N_4$ and N_2 molecule are calculated from the ground-state total energies of the crystals, E_{tot}^{bulk}, and the free atoms, E_{atom_i}, as follows:

$$E_{coh} = E_{tot}^{bulk} - \sum_i E_{tot}^{atom_i}. \quad (12)$$

We should note that in order to calculate the total energy of a free atom using periodic boundary conditions, some technical aspects should be considered. A large cubic supercell is needed to prevent one atom from a certain unit cell from interacting with an atom of a neighboring unit cell. In the calculation of the cohesive energy we include the so-called spin-polarization correction energy for the spin-saturated spherical free (pseudo)atom by adding the difference of the total energies of the spin-polarized and saturated all-electron atom.

III. RESULTS

A. Bulk properties

Here we briefly decribe the bulk properties we calculated for the GaN, Ga-bulk, Si_3N_4, and N_2 molecule. A complete description of these results along with a comparison with other theoretical data is given in Ref. 32.

We have optimized the lattice parameters for GaN in the wurtzite structure, which is the most stable phase of GaN at low temperatures and pressure. Table I shows the results for the calculated bulk properties: lattice constants a_0 and c_0/a_0, bulk modulus B_0, cohesive energy E_{coh}, and formation enthalpy $\Delta H_f^{T=0}$. We find that the LDA underestimates the experimental lattice parameters by around 1%. The cohesive energy is overestimated with respect to the experimental value by 17% and the formation enthalpy by 8% (−1.15 eV).

TABLE III. Calculated and experimental equilibrium lattice constants a_0, c_0/a_0, cohesive energy E_{coh}, and formation enthalpy $\Delta H_f^{T=0}$ for the β-Si_3N_4 using the LDA. The spin-polarization correction for the Si atom is 0.79 eV and for the N atom is 3.03 eV. These values were taken from Refs. 36 and 37.

Ref.	a (Å)	c_0/a_0	B_0 (MBar)	E_{coh} (eV)	$\Delta H_f^{T=0}$ (eV)
This work	7.600	0.383	2.56	−97.91	−9.95
38,39 (Expt.)	7.608	0.382	2.58	−82.96	−8.83

TABLE IV. Calculated and experimental bond length d, binding energy E_b, and vibration frequency ω for an N_2 molecule using the LDA. The binding energy was corrected by a spin-polarization correction of 3.03 eV. This value was extracted from Ref. 36. The zero-point vibration energy of the molecule (0.153 eV) has been included.

Ref.	d (Å)	E_b (eV)	ω (cm^{-1})
This work	1.09	−11.71	2363
40 (Expt.)	1.10	−9.82	2360

We have calculated Si in the diamond structure with two Si atoms in the primitive unit cell. Our calculated properties are shown in Table II, where we compare our results with experimental values. As expected, the LDA predicts a slightly smaller lattice constant (−1%) and a larger cohesive energy (+10%) than the experimental value,

$\beta-Si_3N_4$ has a structure with 14 atoms per unit cell (8 N and 6 Si) and belongs to the point group $P6_3/m$. Each Si atom is tetrahedrally coordinated with one N atom. The N atoms are nearly planarly threefold coordinated with Si. Recent theoretical investigations have shown that this phase is the most stable one at $T=0$ and $P=0$. At $P=42$ atm and T = 1770 K, the β phase transforms into the α phase, which has twice as many atoms per unit cell and a different stacking along the $\{c\}$ direction.[35] The optimized structure and the cohesive properties are shown in Table III and compared with the experimental and data available. Our results for the lattice parameters show very good agreement with experimental values for the structural properties and other theoretical calculations.[36]

The results for the binding energy, bond length, and vibration frequency for the N_2 molecule are shown in Table IV. The vibration frequency is calculated from the total energy versus N_2 bond length. The bond length was varied around the experimental bond length (1.10 Å) ranging from −9% to 9%. Our results are in good agreement with previous LDA calculations using the pseudopotential approach.[36] The binding energy is overestimated by 16% using the LDA. From Table IV we can see that our results compare quite well with experimental values.

Ga bulk has different bulk phases (Ga-II, Ga-III,[41] α,[42] β,[43] γ,[44] δ,[45] and ϵ[41]), depending on the pressure and temperature. Several theoretical and experimental studies have shown that α-Ga is the stable phase at room temperature and low pressure (up to 16×10^3 atm).[46] The α phase has an

TABLE V. Calculated and experimental structural and thermodynamic properties of Ga bulk in the α phase using the LDA: equilibrium lattice constants a_0, b_0/a_0, c_0/a_0, u, and v and cohesive energy E_{coh}. The cohesive energy was corrected by a spin-polarization calculates of 0.145 eV. This value was extracted from Ref. 36.

Ref.	a_0 (Å)	b_0/a_0	c_0/a_0	u	v	E_{coh} (eV)
This work	4.51	1.001	1.695	0.0785	0.1525	−3.29
34 (Expt.)	4.511	1.001	1.695	0.0785	0.1525	−2.81

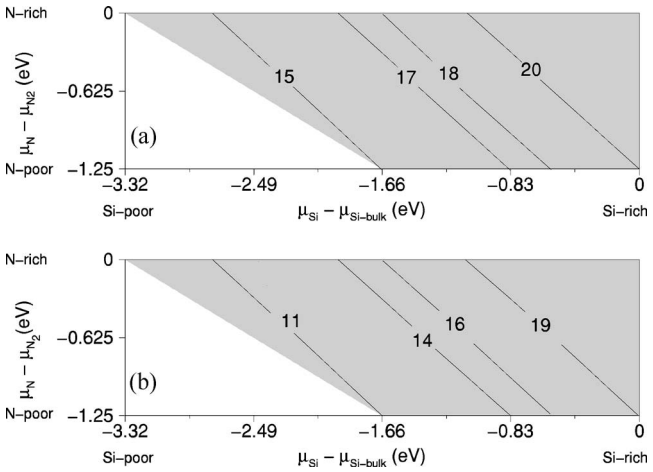

FIG. 1. Si concentration as a function of the Si (μ_{Si}) and N (μ_N) chemical potentials for typical temperatures of (a) MOCVD (1300 K) and (b) MBE (900 K) growth. The solid lines represent the Si concentration given in $\log_{10}\,\mathrm{cm}^{-3}$. The shaded region shows the allowed region where the formation of Si_3N_4 is thermodynamically stable.

orthorhombic structure with eight atoms per unit cell. A peculiar feature is that each atom has only one nearest neighbor at a distance of 2.44 Å. The second, third, and fourth shells each contain two atoms and are 0.27, 0.30, and 0.39 Å farther away. We use the experimental lattice parameters taken from Ref. 46.

The results for the calculated and experimental properties are shown in Table V. The cohesive energy calculated is overestimated by around 15% using the LDA.

B. Si in GaN bulk

In Fig. 1 we plot the Si concentration in GaN bulk as a function of the Si (μ_{Si}) and N (μ_N) chemical potentials for typical temperatures in MBE and MOCVD growth [Eq. (1)]. The concentration increases going from N-poor (Ga-rich) to N-rich conditions if the Si chemical potential is kept constant. The solubility is limited by the formation of Si_3N_4. The region where the system is unstable against Si_3N_4 is marked by the gray area in Figs. 1(a) and 1(b). It is interesting to note that the maximum solubility is achieved under N-poor

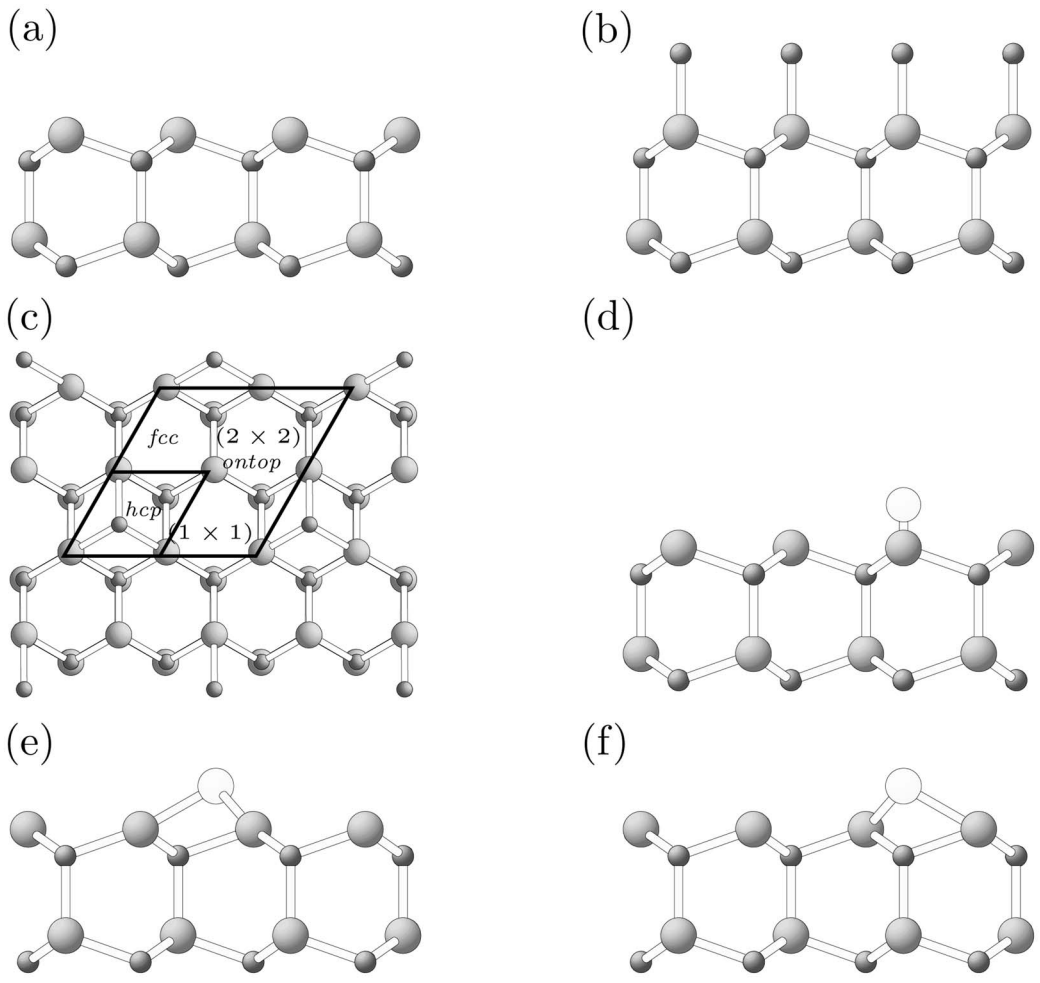

FIG. 2. Side view of the (a) clean Ga-terminated and (b) N-terminated (0001) GaN surfaces. (c) Top view of the (1×1) and (2×2) unit cells of the clean GaN(0001) surface, indicating the highest symmetry adsorption sites fcc, hcp, and on-top. (d) Side view of the Si on-top, (e) Si fcc, and (f) Si hcp structures. The atoms in the first layer are Ga, but can be N as well. White spheres are Si, large grey spheres are Ga and small grey spheres are N.

conditions, because N-rich conditions promote the formation of Si_3N_4.

The maximum Si concentration which can be incorporated in GaN increases with temperature. However, with increasing temperature the Ga vacancy concentration increases and approaches the Si concentration, as shown by Neugebauer and Van de Walle.[15] Since the Ga vacancy is an acceptor, it will partially compensate the Si donors, leading to a saturation in the Si concentration.

C. Si at GaN surfaces

1. Si at clean N- and Ga-terminated surfaces

To study the adsorption of Si at GaN surfaces, we restricted our calculations to (1×1), (2×2) and $(\sqrt{3}\times\sqrt{3})$ surface unit cells. This is justified by noticing that the observed Si-adsorbed structures show these reconstructions depending on the Si concentration.[1] We first place Si adatoms (adsorbed atoms) on the clean Ga- and N-terminated surfaces. The procedure is done as follows: Si atoms have been placed on the fcc, hcp (hollow sites), and on-top positions on the Ga- and N-terminated surfaces, as shown in Fig. 2(c). Considering a (2×2) unit cell, the Si coverage Θ_{Si} assume the values 1/4, 1/2, and 3/4 ML. For $\Theta_{Si}=1$ ML we use an (1×1) unit cell.

In order to determine the stability of the different configurations we calculate the surface energy γ_s as a function of the chemical potentials of the involved atomic species, Ga N, and Si:

$$\gamma_s = E_{tot}^{slab} - \mu_N n_N - \mu_{Ga} n_{Ga} - \mu_{Si} n_{Si}, \tag{13}$$

where E_{tot}^{slab} is the total energy of the slab used to model the surface and μ_N, μ_{Ga}, and μ_{Si} are the N, Ga, and Si chemical potentials, respectively. n_N, n_{Ga}, and n_{Si} are the number of N, Ga, and Si atoms.

Since it is not possible to calculate the absolute surface energy for the GaN(0001) surface due to a lack of inversion symmetry, all calculated surface energies are given with respect to a reference surface energy $\gamma_s^{clean(Ga\ term)}$, which is the surface energy of the clean Ga-terminated surface. Therefore we write the equation above as

$$\gamma_s = E_{tot}^{slab} - \mu_N n_N - \mu_{Ga} n_{Ga} - \mu_{Si} n_{Si} - \gamma_s^{clean(Ga\ term)}. \tag{14}$$

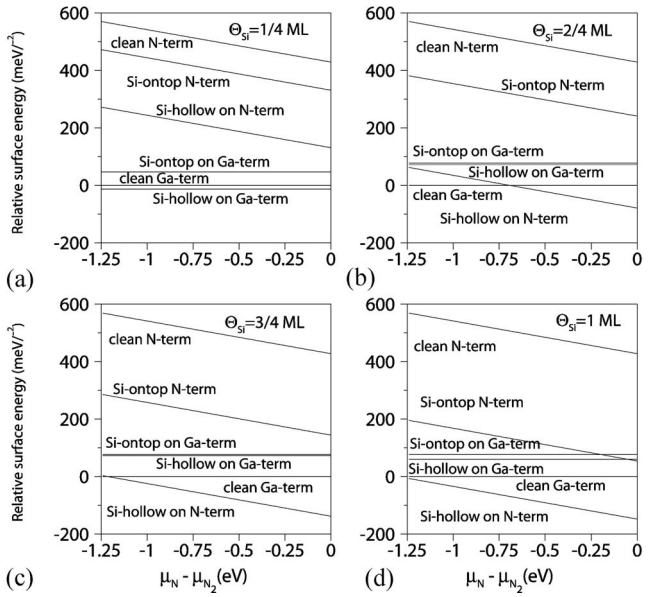

FIG. 3. Relative surface energy for Si adsorbed on the clean Ga- and N-terminated GaN(0001) surface for (a) $\Theta_{Si}=1/4$, (b) $\Theta_{Si}=2/4$, (c) $\Theta_{Si}=3/4$, and (d) $\Theta_{Si}=1$ ML. Si-rich conditions ($\mu_{Si}=\mu_{Si\ bulk}$) are assumed.

In Fig. 3 we plot the relative surface energy as a function of the N chemical potential. The Si chemical for the structures of Fig. 2 potential is set to Si-rich conditions ($\mu_{Si}=\mu_{Si\ bulk}$). We can see that all structures with Si on the clean Ga-terminated surface have a higher surface energy than the clean Ga-terminated surface. This is found for all Si cover-

TABLE VI. Bond lengths d between Si adatoms and substrate atoms (N or Ga) and interlayer spacing between the first and second planes Δz_{12}. Si coverages in the range $1/4 \leqslant \Theta_{Si} \leqslant 1$ ML were considered. As a matter of comparison the Si-N and Si-Ga dimer bond lengths are 1.58 and 2.3 Å, respectively.

	$d_{Si\text{-}N}$ (Å)			Δz_{12} (Å)		
Θ_{Si} (ML)	hcp	fcc	on-top	hcp	fcc	on-top
1/4	1.68	1.68	1.60	0.29	0.30	1.60
2/4	1.70	1.77	1.65	0.30	0.35	1.65
3/4	1.76	1.75	1.64	0.53	0.51	1.64
4/4	2.01	2.02	1.64	0.81	0.83	1.64
	$d_{Si\text{-}Ga}$ (Å)			Δz_{12} (Å)		
Θ_{Si} (ML)	hcp	fcc	on-top	hcp	fcc	on-top
1/4	2.40	2.48	2.30	1.51	1.52	2.30
2/4	2.46	2.46	2.31	1.51	1.51	2.31
3/4	2.52	2.52	2.35	1.69	1.69	2.35
4/4	2.82	2.82	2.47	2.14	2.14	2.47

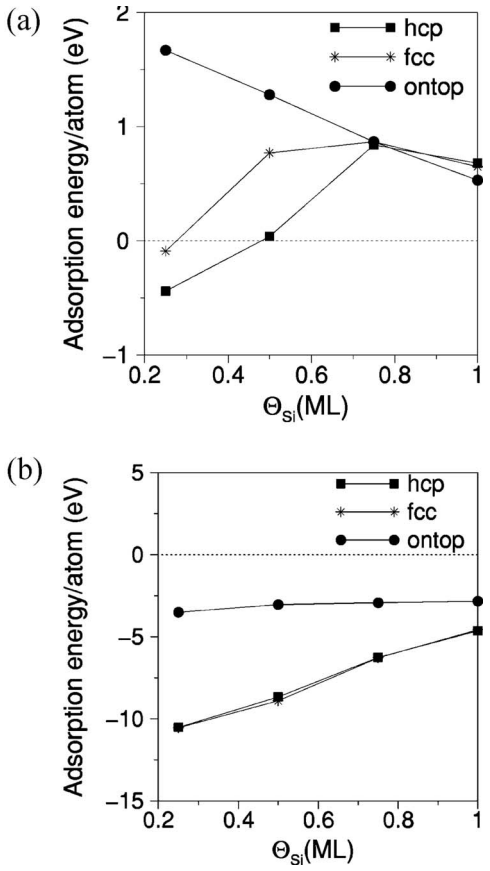

FIG. 4. Adsorption energy calculated according to Eq. (16) of Si on the (a) Ga-terminated and (b) N-terminated GaN(0001) surface for $1/4 \leqslant \Theta_{Si} \leqslant 1$ ML for the fcc, hcp, and on-top sites. The zero of energy is set to the cohesive energy of Si bulk.

ages, regardless of the adsorption site. The only exception is the hollow site for small coverage ($\Theta_{Si}=1/4$), which is energetically more favorable than the clean Ga-terminated surface.

For the N-terminated surface we found that adsorption on the on-top site is energetically unfavorable, regardless of the Si coverage. The hollow hcp and fcc sites are degenerate in energy within the estimated accuracy and become more favorable as the Si coverage increases.

We can therefore conclude that Si strongly prefers the adsorption on N-terminated surfaces rather than on the Ga-terminated surface. Besides, Si prefers to maximize the formation of Si-N bonds. This can be seen noticing that the threefold-coordinated hollow site is preferred rather than the singly coordinated on-top site.

In order to understand why adsorbing Si on the Ga-terminated surface destabilizes the surface while adsorption of Si on the N-terminated surface stabilizes it for high Si coverages, we analyze the bond lengths of Si-N and Si-Ga as a function of the Si coverage for all adsorption sites fcc, hcp, and on-top. As a matter of comparison, we model the strength of single Si-Ga and Si-N bonds by calculating a Si-N dimer and a "fictitious" Si-Ga dimer. The dimers calculations have been performed using a large cubic supercell of 10 Å to avoid interaction between dimers of neighboring cells.

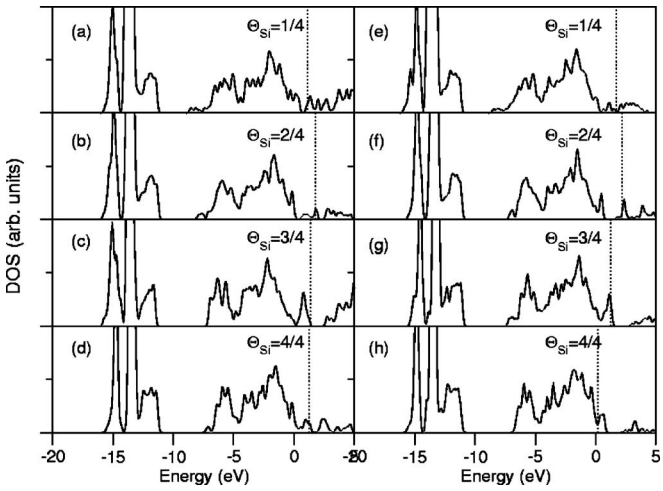

FIG. 5. Total density of states for Si adsorbed on the hcp site of a (a)–(d) Ga-terminated GaN(0001) surface and (e)–(h) N-terminated GaN(0001) surface. Silicon coverages in the range $1/4 \leqslant \Theta_{Si} \leqslant 1$ ML were considered. The dashed vertical line indicates the Fermi level. The zero of energy is set to the top the valence band of GaN bulk.

The optimized bond lengths of these dimers are shown in Table VI. That there is no significant difference between the bond length of a Si-Ga dimer (2.3 Å) and the bond lengths of a Si-Ga with Si is adsorbed on the on-top site of the Ga-terminated surface. For the fcc and hcp sites, the difference between the dimer bond length and the Si-Ga bond length on the surface lies in the range 0.1–0.3 Å. The general tendency is that the Si-Ga bond lengths tend to increase as Θ_{Si} coverage increases.

For the adsorption on the N-terminated surface, we found that there is no significant difference between the Si-N dimer bond length and the Si-N bond lengths on the surface the on-top position (less than 0.1 Å) for $1/4 \leqslant \Theta_{Si}=3/4$ ML. However, for $\Theta_{Si}=1$ ML the difference is slightly larger (0.3 Å). For the hollow sites, the tendency is that the bond length increases as the coverage increases. In particular, for a fully adsorbed monolayer, the bond length is 0.4 Å larger than the bond length of the dimer.

Moreover, as the coordination of Si with the N atoms in the first layer increases, the bond length tends to the bond length of a Si-N bond in Si_3N_4 bulk (1.74 Å) for $\Theta_{Si}=3/4$ ML. We can understand it by noting that in Si_3N_4 bulk Si is tetrahedrally coordinated with N. Thus all three Si atoms at the surface are arranged in a similar tetrahedral configuration as in Si_3N_4 bulk, except that on the surface the Si atoms are only three fold coordinated. For $\Theta_{Si}=1$ ML, however, the Si-N bond length is slightly larger (0.3 Å for the hollow sites and 0.5 Å for the on-top site).

The adsorption energy of an atom, E_{ad}, on a clean surface is written as

$$E_{ad}/N_{adatom} = E_{tot}^{surf+adatom} - E_{tot}^{clean\ surf} - N_{adatom}E_{tot}^{adatom}, \qquad (15)$$

where $E_{tot}^{surf+adatom}$ is the total energy of the surface with the adsorbed atoms, $E_{tot}^{clean\ surf}$ is the total energy of the surface without the adatom (clean surface), and E_{tot}^{adatom} is the total

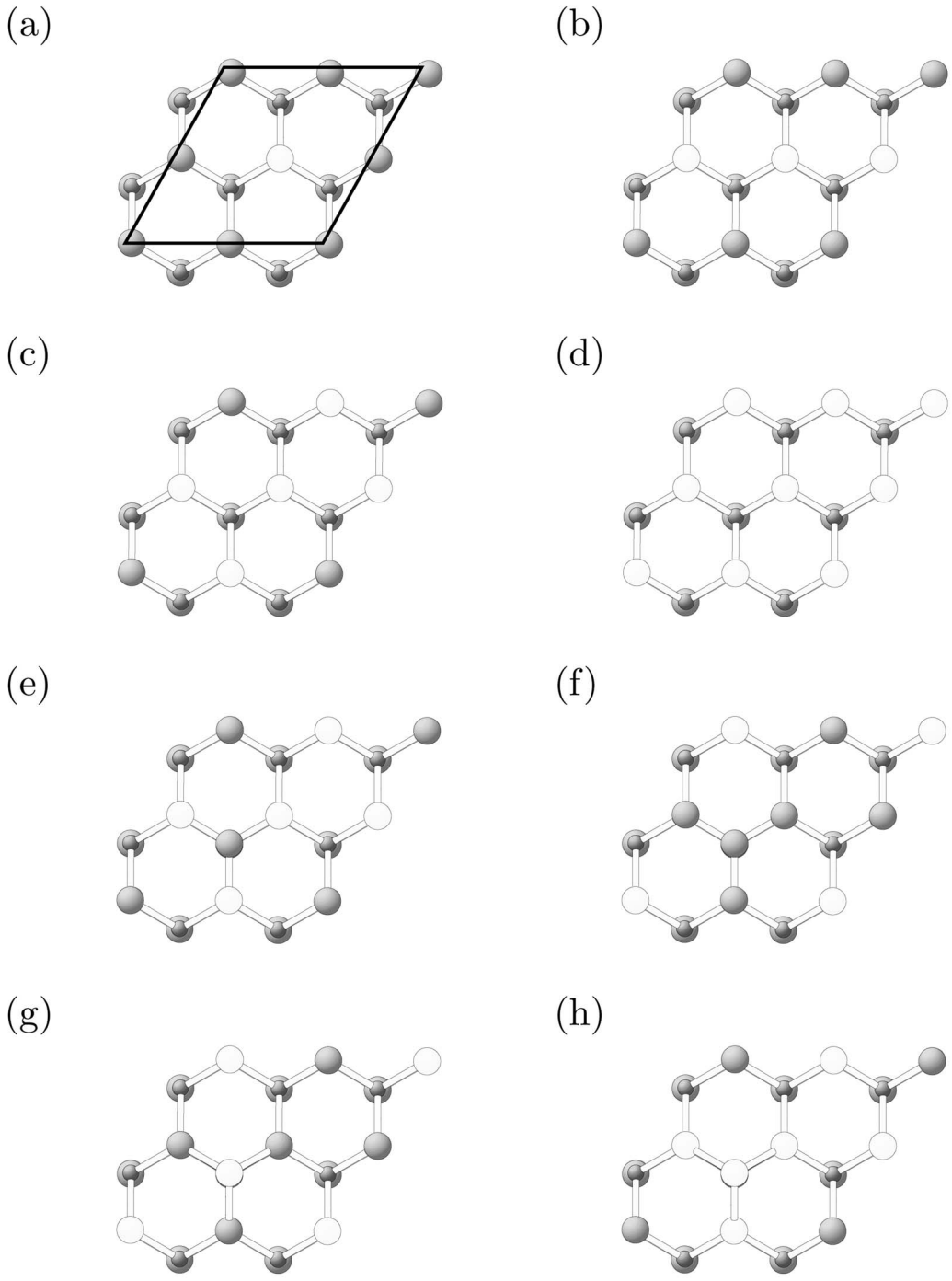

FIG. 6. Top view of the mixed (2×2) surfaces. The starting point to obtain the mixed (2×2) structures is the clean Ga-terminated surface. In (a)–(d) atoms on the first layer are systematically replaced by Si atoms, which leads to surfaces with coverages 1 Si+3 Ga (a), 2 Ga+2 Si (b), 3 Si+1 Ga (c), and 4 Si+0 Ga (d) in the first layer. In (e)–(h) structures with adatoms on the mixed surfaces are shown. (e) Ga adatom on 3 Si+1 Ga, (f) Ga adatom on 3 Ga+1 Si, (g) Si adatom on 3 Ga+1 Si, and (h) Si adatom on 3 Si+1 Ga. White spheres are Si, large grey spheres are Ga, and small grey spheres are N. The surface unit cell is also shown.

energy of the adatom—i.e., of the free atom. For ease of viewing, Eq. (15) is referred with respect to the cohesive energy of Si bulk per atom, $E_{\mathrm{coh}}^{\mathrm{Si\ bulk}}$. Therefore Eq. (15) is written as

$$E_{\mathrm{ad}}^{\mathrm{ref}}/N_{\mathrm{adatom}} = E_{\mathrm{tot}}^{\mathrm{surf+adatom}} - E_{\mathrm{tot}}^{\mathrm{clean\ surf}} - N_{\mathrm{adatom}}E_{\mathrm{tot}}^{\mathrm{adatom}} - E_{\mathrm{coh}}^{\mathrm{Si\ bulk}}, \tag{16}$$

In Fig. 4 we plot the adsorption energy of Si on the Ga- and N-terminated surfaces as a function of Si the coverage. Here we set the zero of energy to the cohesive energy of the bulk phase of Si. If the adsorption energy lies above this zero, adsorption on a specific site is favored. As we can see from Fig. 4(b), the adsorption energy of Si on the N-terminated surface is very large. This can be understood

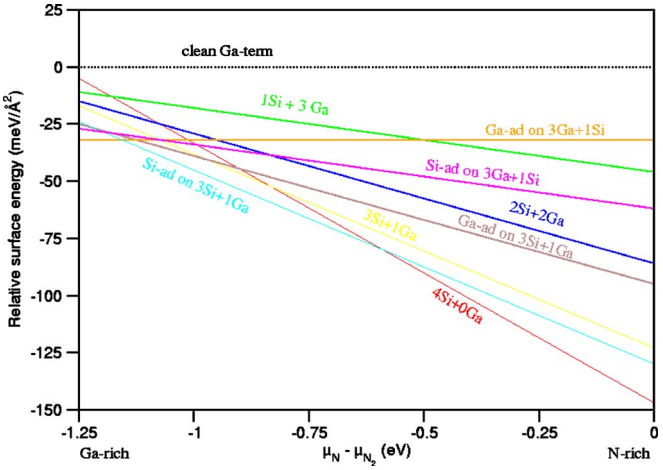

FIG. 7. (Color online) Relative surface energy of the (2×2) mixed surfaces shown in Fig. 6. Si-rich conditions are assumed. The energy zero was set to the clean Ga-terminated surface (dotted line).

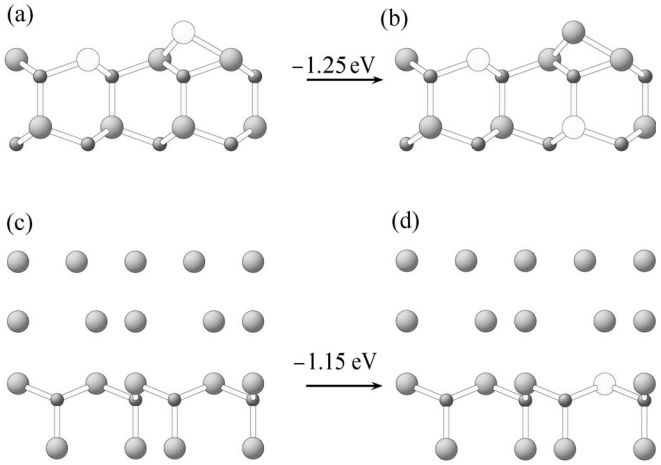

FIG. 8. Change in the energetics of the surfaces depending on the position of the Si atoms for. (a) Si adatom on a surface with 3 Ga and 1 Si atoms in the first layer, (b) Ga adatom on a surface with 3 Ga and 1 Si atoms+1 Si subsurface (third layer), (c) Ga-bilayer structure, and (d) Ga-bilayer structure with Si subsurface (third layer). The energy difference per unit cell between the structures is also indicated.

noticing that the experimental binding energy of a Si-N molecule is rather large (−4.8 eV).[40] As the clean N-terminated surface has three dangling bonds, once one Si atom is adsorbed on this surface, it will form bonds with the N atoms on the surface, leading to a gain of energy of approximately 4.8 eV per bond.

However, clean N-terminated GaN (0001) surfaces are found to be thermodynamically unstable[10] and it might be difficult to prepare a N-terminated surface in order to adsorb Si on it. Adsorption on the hollow (fcc, hcp) site is preferred instead of adsorption on the on-top site. We note that the adsorption energy for the on-top site is approximately the same for all coverages, while adsorption on the hollow site decreases with increasing Si coverage.

Adsorption of Si on the Ga-terminated surfaces leads to a relatively small energy gain compared to the energy gain of Si on the N-terminated surfaces and is favored only for $\Theta_{Si}=1/4$ ML at the hollow site.

The total density of states of Si adsorbed on the hollow site of the clean Ga- and N-terminated surfaces is shown in Figs. 5(a)–5(e) and 5(h), respectively. Si coverages in the range $1/4\leqslant\Theta_{Si}\leqslant1$ ML were considered. In the case of Si adsorbed on Ga-terminated surfaces, we can see that the Fermi level changes slightly with the coverage and *all* surfaces have metallic character.

On the other hand, for Si adsorbed on the N-terminated surfaces the surface changes from a metallic behavior, with states inside the band gap, for $\Theta_{Si}=1/4$ ML [Fig. 5(e)] to an almost semiconducting character for $\Theta_{Si}=1$ ML [Fig. 5(h)]. The Fermi level for $\Theta_{Si}=1$ ML in Fig. 5(h) is pinned at the top of the valence band.

2. Si on mixed Ga- and Si-terminated surfaces

As mentioned above, during Si deposition on GaN surfaces, a (2×2) reconstruction is observed in a narrow range of temperature.[1] To identify a possible candidate for this surface, we have built up surfaces containing Si and Ga atoms with (2×2) periodicity. The question is how to select surfaces with low formation energy among so many possibilities. The electron-counting rule (ECR) states that the surfaces of polar III-V semiconductors should reconstruct such that all the dangling bonds on the electropositive surface atoms (III) are unoccupied and all those on the electronegative atoms (V) are doubly occupied, with the resulting surface band gap similar to that of the bulk. The most prominent application of the electron-counting rule has been to narrow the possible structural models for the many reconstructions observed. It has been shown that it works well for conventional III-V materials, but it is insufficient to explain surface stability in the case of clean GaN surfaces (see, for example, Ref. 47). It is worth noting, however, that Si and Ga atoms have very similar electronegativity. Therefore, the ECR should be used with caution to narrow down the number of possible configurations.

At a first step, we studied structures that contain Ga and Si atoms in the first layer (we call them mixed surfaces). We replace the Ga atoms in the outermost layer by Si atoms in the (2×2) unit cell, as shown in Figs. 6(a)–6(d). By doing so, we obtain surfaces with Ga coverage $0\leqslant\Theta_{Ga}\leqslant1$ ML and Si coverage $0\leqslant\Theta_{Si}\leqslant1$ ML. In addition, we study structures with Ga and Si adatoms on the mixed structures containing 3 Si+1 Ga and 3 Ga+1 Si in the first layer, as shown in Figs. 6(e) and 6(h). By doing so, we have $1/4\leqslant\Theta_{Si}\leqslant1$ ML.

In Fig. 7 we plot the relative surface energy γ_s for the structures discussed above. At N-rich conditions a structure with 4 Si and no Ga atoms in the first layer is more stable (the red line in the graph). This structure is shown in Fig. 6(d). Going towards more Ga-rich conditions a structure with a Si adatom on a surface with 3 Si+1Ga in the top layer is more stable (cyan line in the graph). This surface is sketched in Fig. 6(h). At extreme Ga-rich conditions a structure rich in Ga is energetically favorable in a narrow range of the chemical potential [orange line in the graph and Fig. 6(f)]. From these results we conclude that under N-rich conditions structures rich in Si are preferred, while under Ga-rich conditions

structures with little Si and rich in Ga are preferred.

3. Si at subsurface sites

We will now relax the condition of Si staying at the surface layers and allow incorporation at subsurface sites. As a first set of structures we considered a Si adatom on a Ga-terminated surface where 0 or 1 of the Ga atoms in the Ga surface layer have been replaced by Si atoms. The top view of these structures is the same as shown in Figs. 6(a)–6(d). The only difference is that the structures contain additionaly Si atoms in the third layer.

Under intermediate Ga-rich conditions, we find that the structure with the lowest energy consists of a Si atom in the first layer and a Si atom in the third layer, both replacing Ga atoms. This surface is shown in Fig. 8(b) and is 1.25 eV/(2×2) lower in energy than the original (2×2) adatom structure shown Fig. 8(a). However, this structure is unstable against other structures with a Si subsurface we will discuss next. This might explain why the (2×2) reconstruction experimentally observed is metastable and disappears under anealling.[1]

We have additionally studied Ga-bilayers on the top of Ga-terminated surfaces with Si at subsurface sites. This study is motivated considering that Auger experiments[48] have shown that this (1×1) structure contains 2–3 ML of Ga atoms on the top layers and that Si might be buried underneath. From a topological point of view, this structure is equivalent to the clean (1×1) Ga-bilayer surface observed under Ga-rich conditions.[9,11,49] We have used a $(\sqrt{3}\times\sqrt{3})$ unit cell to model this structure,[50] and it contains between 1/3 and 1 ML of Si at subsurface sites.

Indeed we find a stable structure consisting of a double layer of Ga on a Ga-terminated surface with $\Theta_{Si}=1/3$ ML [see Fig. 8(d)]. This structure is 1.15 eV/$(\sqrt{3}\times\sqrt{3})$ cell lower in energy than the clean contracted Ga bilayer shown in Fig. 8(c). This result suggests that the Ga bilayer observed in the STM images under Ga-rich and Si-rich conditions has Si atoms below the surface.

D. Surface phase diagram and consequences for growth

Among all possible configurations we have investigated, the most stable ones are shown in Fig. 9. In Fig. 10 we show

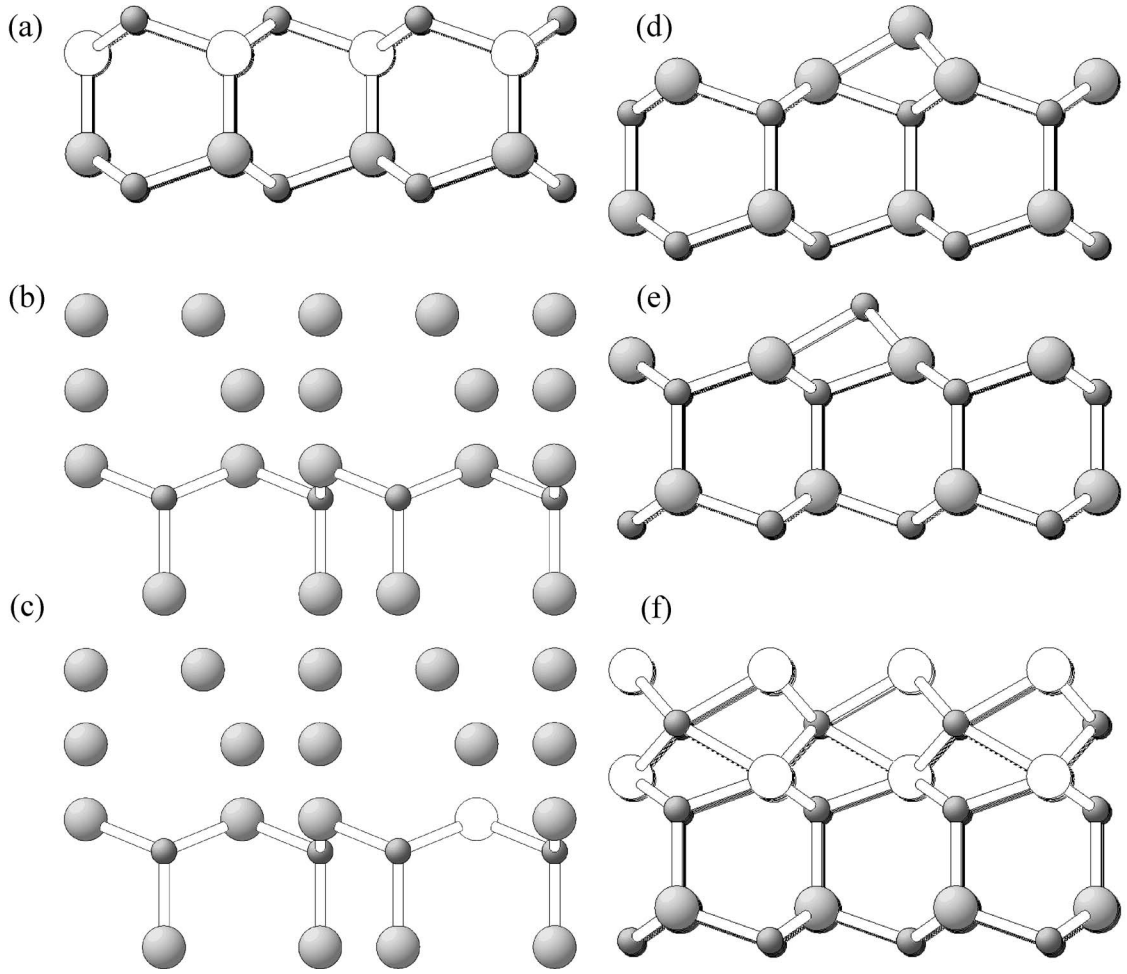

FIG. 9. Atomic geometries of the thermodynamically stable structures. (a) N-terminated surface with Si in the second layer, (b) contracted Ga bilayer, (c) contracted Ga bilayer with Si at subsurface site in the third layer, (d) Ga adatom at the hcp site on the clean Ga-terminated surface, (e) N adatom at the fcc site on the Ga-terminated surface, and (f) 1 ML of Si on the N-terminated surface with 1 ML of Si in the third layer. White spheres are Si, big grey spheres are Ga, and small grey spheres are N.

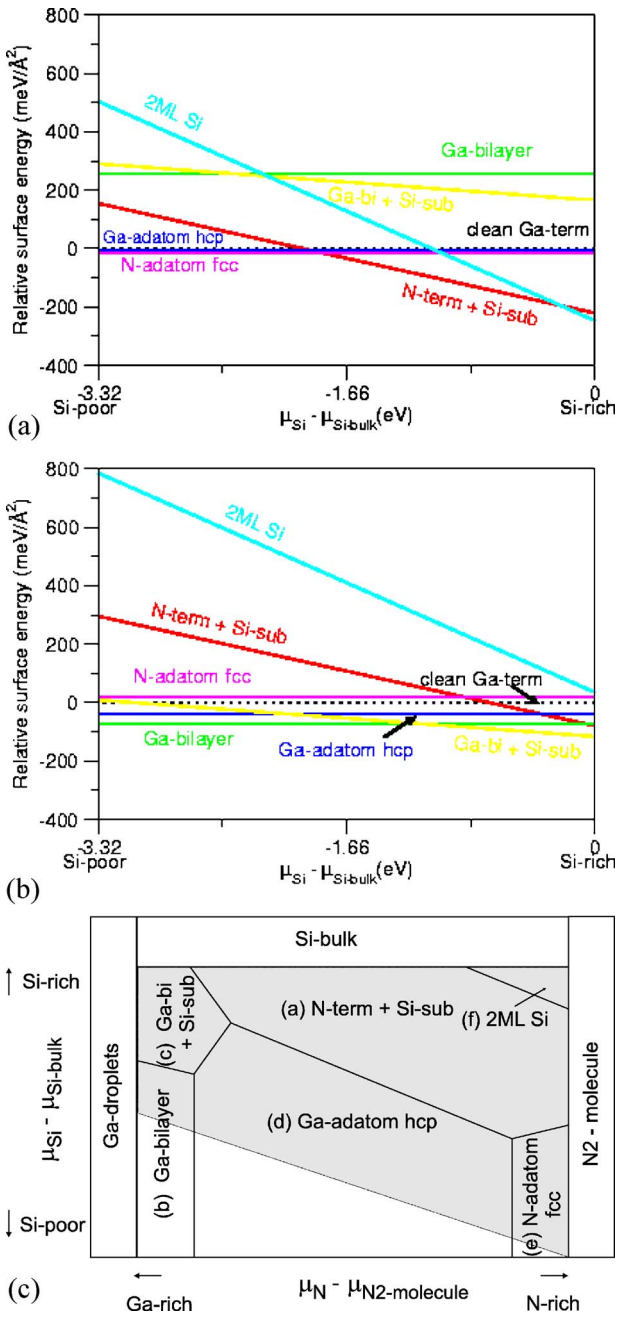

FIG. 10. (Color online) Relative surface energy of the thermodynamically stable structures. (a) N-rich conditions are assumed and (b) Ga-rich conditions are assumed. (c) Growth phase diagram as a function of both Si (μ_{Si}) and N (μ_N) chemical potentials. The shaded area shows the region where all structures are unstable against the formation of Si_3N_4. The atomic geometry of these structures is shown in Fig. 9.

the relative surface energy as a function of μ_{Si}. In Figs. 10(a) N-rich conditions are assumed and 10(b), where Ga-rich conditions are assumed.

Let us first discuss Fig. 10(a), where N-rich conditions are assumed. We can see that under Si-rich conditions, a (1×1) N-terminated structure with Si in the second layer is found to be thermodynamically stable. This structure is shown in Fig. 9(a). Under Si-rich and N-rich conditions, a structure consisting of a full monolayer of Si on a N-terminated surface and 1 ML of Si in the third layer is found to be energetically stable. This structure is shown in Fig. 9(f). Thus, surfaces which form a large number of Si-N bonds are preferred. Going towards less Si-rich conditions, structures with no Si are energetically favorable, as expected. This results are in agreement with Ref. 50, where a N adatom adsorbed at the fcc site of a clean Ga-terminated surface is the most stable surface [see Fig. 9(e)].

Under Ga-rich and Si-rich conditions, as shown in Fig. 10(b), a contracted Ga bilayer containing 1/3 ML of Si residing in the third layer is found to be favored. This structure is sketched in Fig. 9(c). Under less Si-rich conditions, we identify the Ga-bilayer structure as the most stable one. So we can conclude that adsorption at subsurface sites is preferred rather than in the top layers under Ga-rich and Si-rich and N-rich and Si-rich conditions.

The results we have shown in two-dimensional plots in Figs. 10(a) and 10(b) can be put together by building up a three-dimensional surface diagram $\gamma_s(\mu_N, \mu_{Si})$.[1] For ease of viewing, we build up a two-dimensional picture, where the relative surface energy is projected on a plane whose axes are the μ_N and μ_{Si} which is shown in Fig. 10(c). The shaded area shows the region where the structures are unstable against the formation of Si_3N_4.

Based on these results the different behaviors observed in MOCVD and MBE growth modes can be explained. If Si adsorbs on the bare GaN surface, it kicks out surface Ga atoms and induces a (2×2) reconstruction. The excess Ga atoms cluster into islands and form a Ga bilayer with a pseudo (1×1) structure stabilized by Si atoms in the third layer. With increasing Si coverage more and more excess Ga atoms are created and the area covered by the Ga bilayer will increase until it eventually covers the entire surface. Therefore, from the topological point of view, no change in the growth mode occurs and the surface shows the same surface termination as the clean contracted bilayer surface observed under Ga-rich conditions. Thus, we suggest that Ga-rich conditions are the optimum regime to incorporate Si in GaN, as observed in MBE growth.

Under more N-rich and Si-rich conditions the activation barrier to form Si_3N_4 is expected to be rather low. Thus Si_3N_4 islands and precipitates may be formed on the surface, since Si_3N_4 is well known to chemically passivate GaN surfaces and blocking growth.[51] Although all the structures we found are unstable against the formation of Si_3N_4, they might be considered as precursor states for Si_3N_4 formation. Thus, the presence of Si precipitates leads to three-dimensional growth, as observed in MOCVD growth.

From the phase diagram we can deduce further trends for the incorporation of Si on GaN surfaces. As we can see from Figs. 1(a) and 1(b), assuming thermodynamical equilibrium, the Si concentration in GaN is restricted to 10^{15} cm^{-3} for MOCVD and to 10^{11} cm^{-3} for MBE growth. However, we have shown that under more N-rich conditions surfaces much higher Si coverage are found. Therefore, the Si concentration at the surface may be significantly larger than in GaN bulk due to surface segregation perhaps.

IV. CONCLUSIONS

In summary, we have investigated adsorption of Si on GaN(0001) surfaces using density-functional theory. We have found that for adsorption on the outermost layer, Si adsorption on the N-terminated surface is preferred rather than on Ga-terminated surfaces. Besides, Si prefers to form the maximum number of bonds with N atoms.

Relaxing the condition that Si stay on the surface, we have found that adsorption at subsurface sites is energetically favorable compared to adsorption on the top layers. In particular, under Ga-rich conditions a Ga bilayer is formed on the top of a Ga-terminated surface with Si incorporated underneath and thus Si does not affect the GaN surface morphology. Under both N-rich and Si-rich conditions, a N-terminated structure with Si in the second layer is preferred. Under such conditions Si adsorption leads to rough surfaces. Our calculations are in agreement with both MOCVD and MBE growth modes and can explain the variety of effects observed in GaN surfaces exposed to Si adsorption.

*Corresponding author. Electronic address: andreia.luisa@fysik.uu.se

[1] A. L. Rosa, J. Neugebauer, J. E. Northrup, C. D. Lee, and R. M. Feenstra, Appl. Phys. Lett. **80**, 2008 (2002).
[2] S. Nakamura and G. Fasol, *The Blue Laser Diode* (Springer-Verlag, Berlin, 1997).
[3] O. Ambacher, J. Phys. D **31**, 2653 (1998).
[4] G. Mula, C. Adelmann, S. Moehl, J. Oullier, and B. Daudin, Phys. Rev. B **64**, 195406 (2001).
[5] B. Heying, R. Averbeck, L. F. Chen, E. Haus, H. Riechert, and J. S. Speck, J. Appl. Phys. **88**, 1855 (2000).
[6] L. X. Zheng, M. H. Xie, S. M. Seutter, S. H. Cheung, and S. Y. Tong, Phys. Rev. Lett. **85**, 2352 (2000).
[7] C. Adelmann, J. Brault, G. Mula, B. Daudin, L. Lymperakis, and J. Neugebauer, Phys. Rev. B **67**, 165419 (2003).
[8] G. Koblmüller, R. Averbeck, H. Riechert, and P. Pongratz, Phys. Rev. B **69**, 035325 (2004).
[9] A. R. Smith, R. M. Feenstra, D. W. Greve, M.-S. Shin, M. Skowronski, J. Neugebauer, and J. E. Northrup, J. Vac. Sci. Technol. B **16**, 2242 (1998).
[10] A. R. Smith, R. M. Feenstra, D. W. Greve, M.-S. Shin, M. Skowronski, J. Neugebauer, and J. E. Northrup, Surf. Sci. **423**, 70 (1999).
[11] H. Chen, R. M. Feenstra, J. E. Northrup, T. Zywietz, J. Neugebauer, and D. M. Greve, J. Vac. Sci. Technol. B **18**, 2284 (2000).
[12] F. Widmann, B. Daudin, G. Feuillet, Y. Samson, J. L. Rouvière, and N. Pelekanos, Appl. Phys. Lett. **83**, 7618 (1998).
[13] F. Widmann, B. Daudin, G. Feuillet, N. Pelekanos, and J. L. Rouvière, Appl. Phys. Lett. **73**, 2642 (1998).
[14] J. Neugebauer and C. G. V. de Walle, in *Proceedings of the 22nd International Conference on the Physics of Semiconductors*, edited by D. Lockwood (World Scientific, Singapore, 1994), Vol. 3, p. 2327.
[15] J. Neugebauer and C. G. V. de Walle, Adv. Solid State Phys. **35**, 25 (1996).
[16] T. S. Cheng, C. T. Foxon, L. C. Jenkins, S. E. Hooper, D. E. Lacklison, J. W. Orton, B. Y. Ber, A. V. Merkulov, and S. V. Novikov, Semicond. Sci. Technol. **11**, 538 (1996).
[17] W. Götz, N. M. Johnson, C. Chen, H. Liu, C. Kuo, and W. Imler, Appl. Phys. Lett. **68**, 3144 (1996).
[18] S. Tanaka, M. Takeuchi, and Y. Aoyagi, Jpn. J. Appl. Phys., Part 2 **39**, L831 (2000).
[19] A. Cremades, L. Görgens, O. Ambacher, M. Stutzmann, and F. Scholz, Phys. Rev. B **61**, 2812 (2000).
[20] L. T. Romano, C. G. V. de Walle, J. W. A., III, W. Götz, and R. S. Kern, J. Appl. Phys. **87**, 7745 (2000).
[21] E. Dumiszewska, D. Lenkiewicz, W. Strupinski, A. Jasik, R. Jakiela, and M. Wesolowski, Opt. Appl. **35**, 111 (2005).
[22] S. Keller, S. F. Chichibu, M. S. Minsky, E. Hu, U. K. Mishra, and S. P. DenBaars, J. Cryst. Growth **195**, 258 (1998).
[23] A. Munkholm, C. Thompson, M. V. R. Murty, J. A. Eastman, O. Auciello, G. B. Stephenson, P. Fini, S. P. DenBaars, and J. S. Speck, Appl. Phys. Lett. **77**, 1626 (2000).
[24] P. Hohenberg and W. Kohn, Phys. Rev. **136**, B864 (1964).
[25] W. Kohn and L. J. Sham, Phys. Rev. **140**, A1133 (1965).
[26] D. M. Ceperley and B. J. Alder, Phys. Rev. Lett. **45**, 566 (1980).
[27] J. P. Perdew and A. Zunger, Phys. Rev. B **23**, 5048 (1981).
[28] N. Troullier and J. L. Martins, Phys. Rev. B **43**, 1993 (1991).
[29] N. Troullier and J. L. Martins, Phys. Rev. B **43**, 8861 (1991).
[30] M. Fuchs and M. Scheffler, Comput. Phys. Commun. **119**, 67 (1997).
[31] H. J. Monkhorst and J. D. Pack, Phys. Rev. B **13**, 5188 (1976).
[32] A. L. Rosa and J. Neugebauer, Phys. Rev. B (to be published).
[33] *Properties of Group-III Nitrides and EMIS Datareviews*, edited by J. H. Edgar (IEEE, London, 1994).
[34] C. Kittel, *Introduction to Solid State Physics* (Wiley, New York, 1996).
[35] W. Y. Ching, L. Ouyang, and J. D. Gale, Phys. Rev. B **61**, 8696 (2000).
[36] M. Fuchs, J. L. F. DaSilva, C. Stampfl, J. Neugebauer, and M. Scheffler, Phys. Rev. B **65**, 245212 (2002).
[37] M. Fuchs, M. Bockstedte, E. Pehlke, and M. Scheffler, Phys. Rev. B **57**, 2134 (1998).
[38] O. Borgen and H. M. Seip, Acta Chem. Scand. (1947-1973) **15**, 1789 (1961).
[39] J. Liang, L. Topor, A. Navrotsky, and M. Mitomo, J. Mater. Res. **14**, 1959 (1999).
[40] *Handbook of Physics and Chemistry*, 76th ed., edited by D. R. Lide (New York, New York, 1995).
[41] L. Bosio, J. Chem. Phys. **68**, 1221 (1978).
[42] R. W. G. Wyckoff, *Crystal Structures* (Wiley, New York, 1962), Vol. 1, p. 22.
[43] L. Bosio, A. Defrain, H. Curien, and A. Rimsky, Acta Crystallogr., Sect. B: Struct. Crystallogr. Cryst. Chem. **25**, 995 (1969).
[44] L. Bosio, H. Curien, M. Dupont, and A. Rimsky, Acta Crystallogr., Sect. B: Struct. Crystallogr. Cryst. Chem. **28**, 1974 (1972).
[45] L. Bosio, H. Curien, M. Dupont, and A. Rimsky, Acta Crystal-

logr., Sect. B: Struct. Crystallogr. Cryst. Chem. **29**, 367 (1973).
[46] M. Bernasconi, G. L. Chiarotti, and E. Tosatti, Phys. Rev. B **52**, 9988 (1995).
[47] T. Zywietz, J. Neugebauer, and M. Scheffler, Appl. Phys. Lett. **73**, 487 (1998).
[48] C. D. Lee, R. M. Feenstra, A. L. Rosa, J. Neugebauer, and J. E. Northrup, J. Vac. Sci. Technol. B **19**, 1619 (2001).
[49] M. M. Sung, J. Ahn, V. Bykov, J. W. Rabalais, D. D. Koleske, and A. E. Wickenden, Phys. Rev. B **54**, 14652 (1996).
[50] J. E. Northrup, J. Neugebauer, R. M. Feenstra, and A. R. Smith, Phys. Rev. B **61**, 9932 (2000).
[51] H. Lahrèche, P. Vennèguès, B. Beaumont, and P. Gibart, J. Cryst. Growth **205**, 245 (1999).